Model-Invariant Hybrid Computations of Separated Flows for RCA Standard Test Cases

Stephen Woodruff
NASA Langley Research Center, Hampton, VA 23681 *

NASA's Revolutionary Computational Aerosciences subproject has identified several smooth-body separated flows as standard test cases to emphasize the challenge these flows present for computational methods and their importance to the aerospace community. Results of computations of two of these test cases, the NASA hump and the FAITH experiment, are presented. The computations were performed with the model-invariant hybrid LES-RANS formulation, implemented in the NASA code VULCAN-CFD. The model-invariant formulation employs gradual LES-RANS transitions and compensation for model variation to provide more accurate and efficient hybrid computations. Comparisons revealed that the LES-RANS transitions employed in these computations were sufficiently gradual that the compensating terms were unnecessary. Agreement with experiment was achieved only after reducing the turbulent viscosity to mitigate the effect of numerical dissipation. The streamwise evolution of peak Reynolds shear stress was employed as a measure of turbulence dynamics in separated flows useful for evaluating computations.

Nomenclature

LES	Large-Eddy Simulation
RANS	Reynolds-Averaged Navier-Stokes
DES	Detached-Eddy Simulation
SST	Shear-Stress Transport
DNS	Direct-Numerical Simulation
C_{DES}	Turbulence model constant
q	A typical flux variable
c	NASA hump chord
h	FAITH bump height
U_∞	Freestream velocity
k	Modelled turbulent kinetic energy
P	Turbulent kinetic energy production
p	Pressure
Re	Reynolds number
μ	Molecular viscosity
μ_t	Turbulence viscosity, $\mu_t = \rho k/\omega$
S_{ij}	Symmetric part of velocity gradient tensor
$\tilde{S}_{ij}$	Model-invariant S_{ij}
s	Model sensitivity variable
t	Time, non-dimensionalized by c/U_∞
$\mathbf{v}$	Velocity vector, non-dimensionalized by U_∞
$\mathbf{x} = (x, y, z)$	Streamwise, normal and spanwise coordinates, non-dimensionalized by chord
β^*	Turbulence model constant
γ	Turbulence model constant
Δ	Mesh size for turbulence model, $\Delta = (\Delta_x \Delta_y \Delta_z)^{1/3}$
$\Delta_x, \Delta_y, \Delta_z$	Mesh sizes in the three coordinate directions

*Research Scientist, Computational Aerosciences Branch

λ	Model blending parameter (function of $\mathbf{x}, t$)
ρ	Density
σ_k	Turbulence model constant
σ_ω	Turbulence model constant
ω	Modelled omega (inverse turbulence time scale)
ϵ	Turbulence dissipation
$\ell_H, \ell_{\text{RANS}}, \ell_{\text{LES}}$	Turbulence length scales (hybrid, RANS and LES)
$\tilde{\partial}_t$	Model-invariant time derivative
$\tilde{\nabla}$	Model-invariant gradient operator

I. Introduction

Smooth-body separation is an important and difficult problem for computational fluid dynamics. It is a prime opportunity for hybrid LES-RANS techniques, because pure RANS computations often fail to predict such flows adequately.[1] The importance of these flows to NASA and the aerospace industry motivated NASA's Revolutionary Computational Aerosciences subproject to select several smooth-body separation test cases as standard cases for study. The present work considers the NASA hump[2] and FAITH[3] test cases, both of which have been studied experimentally and computationally.

The challenge of smooth-body separation prediction is addressed here with the model-invariant hybrid formulation,[4–6] which seeks to provide a seamless and accurate transition between LES and RANS regions in a hybrid computation. Doing so will enable significantly more efficient hybrid computations by reducing computationaly expensive LES regions to only those parts of the flow where RANS modelling cannot provide an adequate representation of the turbulence dynamics. The model-invariant formulation has been implemented in the finite-volume CFD code VULCAN-CFD[7] for this work, which additionally provides the opportunity of identifying and addressing the problems inherent in adapting a RANS code to LES use.

Model invariance is defined[4,5] as the property that physical quantities in a hybrid computation are unchanged by variations in the split between the RANS and LES parts of the blended hybrid model. Two measures may be taken in a model-invariant computation to ensure this property holds: the transition between RANS and LES models may be made gradually (in contrast to the rapid or instantaneous transitions of DES and other common approaches) and the equations may be modified to eliminate spurious contributions to derivatives due to the changing model. In some cases, the placement and width of the transition is such that the second measure is not necessary; this is true of the present computations.

Earlier examinations of LES-RANS blending followed four paths. In one, the blending function defining the LES-RANS mix at a given point in the flow is determined to reduce log-layer mismatch. IDDES[8] is the most prominent example of this approach; the authors of Refs. 9 and 10 position the transition layer to achieve a similar effect. The second path involves explicit random forcing at the LES-RANS interface.[11–13] Ref. 13 combines this strategy with IDDES. The third path blends RANS time or ensemble averages and LES spatial filters.[14,16–19] This approach employs the derivative expressions described below, but ad hoc modelling is required to specify the new terms that appear in these expressions. The present formulation provides a theoretical basis for their determination. The fourth path directly modifies the turbulent viscosity to account for resolved stresses.[20–23]

The two test cases examined in the present work are the NASA hump and FAITH experiments. The NASA hump was conceived as a convenient configuration for the experimental and CFD investigation of smooth-body separation from airfoil surfaces.[24] The configuration consists of an airfoil-shaped hump mounted on the bottom surface of a channel. Flow control is provided by a synthetic jet mounted on the after part of the airfoil surface, but only the non-flow-control baseline case will be considered here. Experiments were performed by Greenblatt et al.[2] at the NASA Langley Research Center. First and second velocity-moment profiles are available at the center plane in a region containing the separation bubble. This flow has been the subject of quite a few RANS, LES and hybrid computations, including Refs. 13 and Refs. 25–31.

The FAITH experiment[3] involves smooth-body separation from an axisymmetric bump on the floor of a wind tunnel. Experimental results include mean velocity profiles at several stations ahead and behind the bump, surface shear stresses and first and second velocity moments in a centerline plane containing the separation bubble. It is much newer than the hump experiment, but even so it has been treated both by RANS[33,34] and DES.[35]

More explanation of the model-invariant formulation is provided in the next section. After that, numerics are discussed, particularly the new features implemented in VULCAN-CFD for the present computations. Then configurations and grids for the NASA hump and FAITH test cases are described, followed by a presentation of the results of the computations. The paper ends with a discussion of implications of those results.

The computations presented here show that good results may be obtained on fairly coarse grids using the model-invariant formulation. However, CFD codes that originated as second-order RANS codes require significant modification to reach levels of accuracy appropriate for LES computations.

II. Model-Invariant Hybrid Computations

The model-invariant formulation for hybrid LES-RANS computations was developed to address difficulties in hybrid computations connected with the "grey area," the transitional region between LES and RANS portions of the flow where the physics is not quite either and significant errors are introduced into the computation. The most commonly identified consequence of these errors is the "log-layer mismatch,"[36] which occurs when the LES-RANS transition is placed in the log layer of a wall-bounded shear layer and the RANS and LES velocity profiles fail to match. A less obvious consequence is the need to expend unnecessary computing resources doing LES in parts of the flow where RANS works fine, simply to avoid placing a RANS-LES transition where its errors will damage results.

The present approach seeks to make a gradual, controlled, transition between LES and RANS regions. It thus makes use of the continuous modeling concept proposed by Speziale.[37] This is in contrast to most blended hybrid models in use today, such as DES,[38] for which the transition is discontinuous, and IDDES,[8] for which it is continuous but explicitly constructed to be as rapid as possible. The intention in the present work is that the gradual transition will permit the flow at each location to adjust itself to the change in model, eliminating the "grey area" that occurs when the transition in the model is made too rapidly and the flow evolves unphysically as it catches up.

The use of a gradual transition raises the question of how to interpret the flow variables in the transition region, where the model and the flow are "somewhere in between" pure RANS and pure LES. This question was addressed in previous papers,[5,6] where it was proposed that the answer lies in recognizing that physical quantities cannot depend on the LES-RANS mixture of the model. Such quantities were called "model invariants."

Physical quantities predicted by both RANS and LES are limited to the first and second moments of the physical variables that appear in RANS. The first moments, averages, like the averaged velocities, are naturally expected to be the same regardless of whether the quantity being averaged is in the RANS region, the LES region or somewhere in the transition region. Second moments are modeled in both LES and RANS, but to different degrees; so one has to construct the corresponding model invariants as combinations of the contribution of the resolved scales and the modeled and unmodeled contributions of the unresolved scales. An example of a second-moment model invariant is the turbulent kinetic energy, which is approximated here simply as the sum of the resolved turbulent kinetic energy and the modeled turbulent kinetic energy.

In previous work,[5,6] it was demonstrated that model invariants are not preserved as the flow evolves. This is because the change in the LES-RANS mixture of the blended model across a LES-RANS transition leads to changes in the flow variables that contribute to the gradients of those variables. These contributions are artifacts of the blended model and have nothing to do with the physical balances in the equations of motion; thus they represent errors in the equations and lead to errors in the solutions to the equations. If these contributions are removed, however, the physical balances of the equations are restored and correct solutions result.

The control-volume formulation of the governing equations provides a convenient means for understanding how these contributions may be removed. For simplicity, only a single direction is considered. An alternative derivation based on a transformation between the actual computation with variable blending of the RANS and LES models and a corresponding computation with a constant blending parameter is given in earlier work.[5,6]

The blended hybrid LES-RANS model contains a blending parameter, λ, which varies between 0 (giving a pure RANS model) and 1 (giving a pure LES model). The blending parameter is a function of space and time and thus defines the LES, RANS and transition zones. It may be defined explicitly prior to the computation or it may be defined in terms of flow quantities, so that the various zones are determined as

part of the computation.

Suppose, then, that some flux component $q(x,s)$ is oriented in the x direction and an infinitesimal control volume has faces of area $dydz$ perpendicular to the x axis at x and $x+dx$. The variable s is used to represent the dependence of q on the model blending; that is, a hybrid computation results when s is set equal to a specific blending parameter λ : $s = \lambda(\mathbf{x},t)$. Then, in the usual fashion, one would conclude that the contribution from this flux is

$$dydz[q(x+dx,s) - q(x,s)] \approx \frac{\partial q(x,s)}{\partial x} dxdydz. \tag{1}$$

If one follows the standard hybrid practice and simply allows the model blending parameter $s = \lambda(\mathbf{x},t)$ to be a function of space and time, the control-volume analysis is unchanged and one arrives at the usual equations, now containing the variable blending parameter. If, on the other hand, one supposes that λ is constant in each infinitesimal control volume, as one generally assumes turbulence model constants to be, and lets λ change only at the interfaces between control volumes, one has an expression with two terms, the first similar to Equation 1 above and the second representing the change due to the jump in λ at the interface at $x+dx$:

$$\begin{aligned} dydz[q(x'+dx',\lambda) - q(x',\lambda)] \quad &+ \quad dydz[q(x'+dx',\lambda+d\lambda) - q(x'+dx',\lambda)] \\ &\approx \quad \left[\frac{\partial q}{\partial x'}dx + \frac{\partial q}{\partial s}d\lambda\right] dydz \\ &\approx \quad \left[\frac{\partial q}{\partial x'} + \frac{\partial q}{\partial s}\frac{\partial \lambda}{\partial x'}\right] dxdydz \end{aligned} \tag{2}$$

Here, x' has been used to represent the change in x within the control volume (i.e. with λ constant). The jump in λ at the interface $x+dx$ is $d\lambda = \partial\lambda/\partial x\ dx$. (The jump could equally well be put at the left interface, x, or split arbitrarily between the left and right interfaces, without changing the result.)

Equating this new expression for the flux, Equation 2, with the usual one, Equation 1, for the flux across the entire control volume, yields an expression for the derivative that was first proposed in the context of hybrid LES-RANS models by Germano.[14] Since the same argument may be applied to the other coordinate directions and to temporal derivatives, expressions for time and space derivatives may be written

$$\frac{\partial}{\partial t'} = \tilde{\partial}_t \equiv \frac{\partial}{\partial t} - \frac{\partial \lambda}{\partial t}\frac{\partial}{\partial s} \qquad \text{and} \qquad \nabla' = \tilde{\nabla} \equiv \nabla - (\nabla\lambda)\ \frac{\partial}{\partial s} \tag{3}$$

(∇' is the gradient operator on the primed variables). The new terms in these expressions cancel out the unphysical gradients caused by the variation of λ.

This procedure illustrates how seemingly minor differences in the manner in which the blended model is applied in the control volume leads, in the limit, to important differences in the governing differential equations. It shows that the present interpretation may be viewed as the continuous limit of a zonal approach, in which each control volume is a zone employing the blended model at a different constant value of λ. This analysis also suggests how model-invariant equations appropriate for finite-volume and other domain-oriented numerical methods (multi-domain spectral methods, finite-element methods, etc.) may be derived directly, as opposed to the discretization of the governing differential equations employed here.

The above expressions for the derivatives are applied to the equations of motion to give the model-invariant form of those equations. To illustrate, the turbulence-model equations are presented, which also provides an opportunity to define the model used in the present computations. The basis for the present hybrid model is Strelets' DES hybrid model,[39] which is in turn based on Menter's SST model,[40]

$$\begin{aligned} \rho\tilde{\partial}_t k + \rho(\mathbf{v}\cdot\tilde{\nabla})k &= P - \rho\epsilon + \tilde{\nabla}\cdot\left[\left(\frac{\mu}{Re} + \sigma_k\mu_t\right)\tilde{\nabla}k\right] \\ \rho\tilde{\partial}_t \omega + \rho(\mathbf{v}\cdot\tilde{\nabla})\omega &= \rho\frac{\gamma}{\mu_t}P - \beta\rho\omega^2 + \tilde{\nabla}\cdot\left[\left(\frac{\mu}{Re} + \sigma_\omega\mu_t\right)\tilde{\nabla}\omega\right]. \end{aligned} \tag{4}$$

The production P is expressed as $P = \mu_t\tilde{S}_{ij}\tilde{S}_{ij}$, where $\tilde{S}_{ij}$ is the symmetric part of the tensor $\tilde{\nabla}\mathbf{v}$. Only the $k-\omega$ branch of the model is used, since the applications of interest here involve transition to LES before the $k-\epsilon$ branch becomes active. Standard values of the $k-\omega$-model constants[40] are used.

The dissipation, ϵ, is given in terms of a hybrid length scale ℓ_H as $\epsilon = k^{3/2}/\ell_H$. Strelets' DES expression for the hybrid length scale[39] was $\ell_H = \min(\ell_{\text{RANS}}, \ell_{\text{LES}})$, where $\ell_{\text{RANS}} = k^{1/2}/\omega$ and $\ell_{\text{LES}} = C_{DES}\Delta$. In the

present work, the hybrid length scale is defined by $1/\ell_H = (1-\lambda)/\ell_{\mathrm{RANS}} + \lambda/\ell_{\mathrm{LES}}$, with λ defined in Section V as a function of position to give a gradual transition between ℓ_{RANS} and ℓ_{LES}. Blending the inverse length scales effectively blends the individual RANS and LES expressions for the dissipation, which has worked well in previous work, but there is no reason the length scales themselves or an arbitrary function of the length scales could not be used.

The model sensitivities (the derivatives of the flow variables with respect to s appearing in Equation 3) must be specified so that the model-invariant equations of motion may be solved. Some simple reasoning yields a crude approximation that has been successful for both plane channel-flow turbulence[5] and periodic-hill flow:[6] All turbulence energy that gets dissipated ultimately gets dissipated by the dissipation term in the kinetic energy equation, regardless of the LES-RANS mix; so the dissipation is a model invariant and its derivative with respect to s is zero. The same reasoning may be applied to the ω equation. Combining these results, one finds $\omega_s = 0$ and k_s is a function of k and $\ell_{\mathrm{RANS}}/\ell_{\mathrm{LES}}$. The derivative of the approximate model invariant $\rho k + \rho|\mathbf{v}|^2/2$ (the total kinetic energy) with respect to s should be (approximately) zero, giving a relation between k_s and the derivative of the velocity magnitude. One ought then to construct model invariants from components of the Reynolds stress tensor to get the derivatives of the individual components of the velocity vector; but, in this very crude approximation, it is assumed that the component normal to the transition zone is 70% of the velocity magnitude, the spanwise tangential component is 30% of the velocity magnitude and the streamwise tangential component is zero. The same values were used for the channel-flow computations of Ref. 5 and the periodic-hill computations of Ref. 6.

III. Numerics

NASA's VULCAN-CFD[7] is a finite-volume code for solving the Navier-Stokes equations with turbulence models and chemical kinetics. It has been extensively used for hybrid LES-RANS computations (e.g., Refs. 41 and 42) and in addition to low-dissipation inviscid flux schemes, it includes a hybrid advection scheme for the inviscid terms, which mixes 4th- or 6th-order central differences with a dissipative scheme for even lower overall dissipation. In spite of this, it was found that in the present application numerical dissipation prevented the proper level of fluctuations from being maintained in the LES part of the flow and additional measures were required to avoid the prohibitive cost of an extremely fine grid.

The over-riding goal of a RANS solver is robustness, which is achieved, at least in part, by adding numerical dissipation. This is contrary to the needs of an LES computation, where sufficient accuracy to generate and maintain fluctuations is essential. Consequently, dissipative contributions to the inviscid fluxes were eliminated and the fluxes computed by 4th- or 6th-order central finite differences. Solution filtering[43] was added to maintain numerical stability. This implicit filtering of the solution was implemented in a block-by-block fashion, so as to avoid increasing inter-processor communications. The viscous terms and the derivatives in the turbulence source terms remain second order. These changes to the inviscid-term computations made significant improvements, but it will be seen when the results are examined that problems remained.

All model-invariant computations described in the results section were performed with fourth-order central differences and sixth-order implicit solution filtering. The standard DES computation described in that section was performed with VULCAN-CFD's fourth-order hybrid advection scheme, since subiteration convergence of the Newton time-advancement scheme could not be maintained when DES was used with solution filtering.

A characteristics-based outflow boundary condition[44] was found to be necessary to reduce reflections from the outflow boundary sufficiently to maintain numerical stability. This boundary condition was implemented by using the linearized, one-dimensional, flow equations to propagate flow quantities from the solution domain to the ghost points on the outflow boundary.

The ability to add small, uniformly-distributed, random velocity perturbations at the inflow boundary was also added, as inflow perturbations have been used successfully in previous hybrid computations to initiate fluctuations (e.g., Ref. 35). It will be seen in Section V that this approach was not successful in the present work.

IV. Configurations and Grids

Details about the computational domains, grids and parameters for the NASA hump and FAITH test cases are provided in this section.

IV.A. NASA Hump

The computational domain for the NASA hump is based on the experimental configuration. The chord of the airfoil hump shape is c. The height and width of the domain are $0.9c$ and $.121c$, respectively. (The width is that employed in Ref. 27.) The domain extends $42.14c$ upstream of the airfoil leading edge, a distance that permits the developing boundary layer on the lower surface to reach the correct thickness when it reaches the airfoil.[24] Linearized characteristic boundary conditions are applied at the ouflow boundary of the domain, $2.0c$ downstream from the airfoil leading edge. (This outflow boundary position was used in Ref. 28.) The upper boundary of the domain is flat, except for a small depression[24] that approximately reproduces the effect of a constriction in the sidewalls of the experimental configuration.[2] Periodic boundary conditions are applied at the channel sides. The Reynolds number based on c is 9.36×10^5.

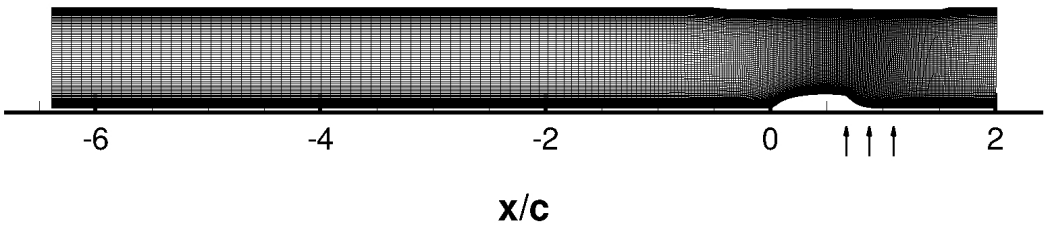

Figure 1. Full grid for NASA Hump. Arrows mark locations of mean-velocity and Reynolds-stress profiles presented below.

The $304 \times 130 \times 20$ grid employed for the hump computation is shown in Figure 1. Significant stretching occurs in the streamwise direction, particularly from the inflow boundary to the hump. The concentration of grid points in the neighborhood of the separation bubble may be seen in Figure 2. Roughly one quarter of the total number of streamwise grid points are contained in that neighborhood. Typical stretching for a viscous flow solution was employed in the wall-normal direction, with the first grid point from the lower wall at $y^+ \approx 1$ or smaller according to a preliminary RANS computation. The spanwise distribution of points is uniform and quite coarse, consistent with the placement of the LES-RANS transition fairly far from the wall, where only larger turbulent structures are present and need to be resolved.

The freestream Mach number was set at 0.25 and a time step of $4.3 \times 10^{-4}\ c/U_\infty$ was found to reduce the subiteration residual by two orders of magnitude.

IV.B. FAITH

As in the case of the NASA hump, the computational domain for the FAITH configuration is based on the experimental setup. The height of the bump is h and its shape is given by a cosine function. The upper wall of the tunnel is $16/3h$ above the floor and the width of the test section is $4.1h$. Periodic boundary conditions are applied at the sides of the domain. The inflow boundary is $40.1h$ upstream of the bump center; this is sufficient to provide for the natural development of the boundary layer to the appropriate thickness. The computational domain extends $100.0h$ downstream of the bump center; the linearized characteristic boundary condition is applied at the outflow boundary. The Reynolds number based on the hump height h is 5×10^5.

The grid (Figure 3) is composed of three blocks laid end to end, of dimensions $50 \times 61 \times 131$, $141 \times 71 \times 131$ and $80 \times 141 \times 131$. Significant streamwise stretching takes place in the upstream and downstream end blocks, while points in the central block, containing the bump, are highly concentrated. As in the case of the hump, the wall-normal spacing was fixed using a preliminary RANS computation and a typical viscous-flow stretching rate.

The freestream Mach number here was also 0.25 and a time step of $2.8 \times 10^{-4}\ h/U_\infty$ yielded two orders of magnitude of subiteration residual reduction.

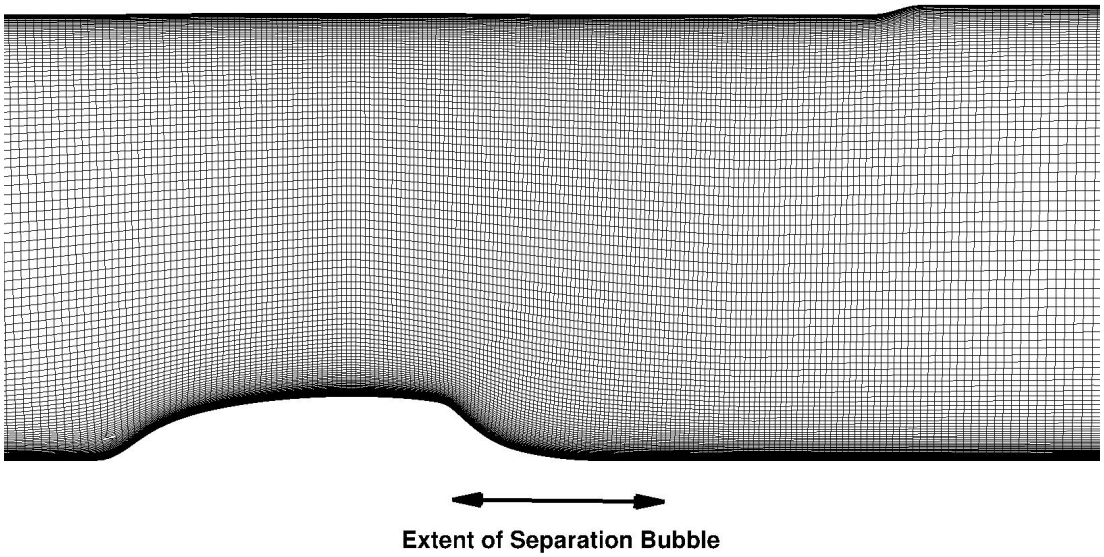

Figure 2. Hump grid clustering in region of separation bubble.

V. Results

Unless otherwise specified, all results displayed are averages. In the case of the NASA hump, averages are over the spanwise, homogeneous, direction and over a time span of 30 c/U_∞. The simulations evolved over a similar time period before averaging began to ensure a statistically steady state had been reached. In the case of the FAITH configuration, averages are over a time span of 30 h/U_∞, with similar precautions to ensure statistical reliability.

Computations of the NASA hump were performed with the LES-RANS transition zone starting at $0.0077c$ from the wall and ending at $0.1024c$ from the wall. Across this zone, the blending parameter λ varies according to a cubic spline from zero to one, with zero derivatives at the edges. The height of the zone places the LES-RANS transition in the middle to outer part of the wall boundary layer; its extreme width makes that transition very gradual.

A straightforward computation of the NASA hump configuration without random forcing at the inflow boundary gives very poor results (Table 1), either with the present approach (Case 2) or standard DES (Case 1). The separation bubbles are too large and turbulence levels within the bubbles are too low, particularly in the upstream portion (Figures 4–6). This behavior is typical of hybrid methods applied to this type of problem. One may see it, for example, in the Reynolds shear-stress profiles provided in Ref. 27 for the hump problem and the Reynolds shear-stress contour plots provided in Ref. 35 for the FAITH problem.

In a parallel investigation, a code employing fourth-order finite-difference and spectral discretizations has been used with the same grid to solve the hump problem successfully with random perturbations applied to the inflow velocities. Applying similar perturbations in VULCAN-CFD failed to have much effect, with results similar to those of Case 2. Efforts to adjust filtering, refine the grid and so on to further reduce dissipation failed to improve matters.

It was discovered that significantly reducing the DES model constant C_{DES} does permit successful computations to be carried out. Reducing C_{DES} increases the dissipation term in the turbulent kinetic energy equation (Equation 4), reducing k and the eddy viscosity $\mu_t = \rho k/\omega$. This in turn reduces the dissipation created by the turbulence model, compensating for the excess numerical dissipation.

In fact, setting up the computation in this way eliminated the need for random forcing at the inflow boundary. As in many applications of DES (such as Ref. 45), fluctuations are generated naturally; it is likely that the reduced dissipation from the reduced C_{DES} also causes some destabilization of parts of the

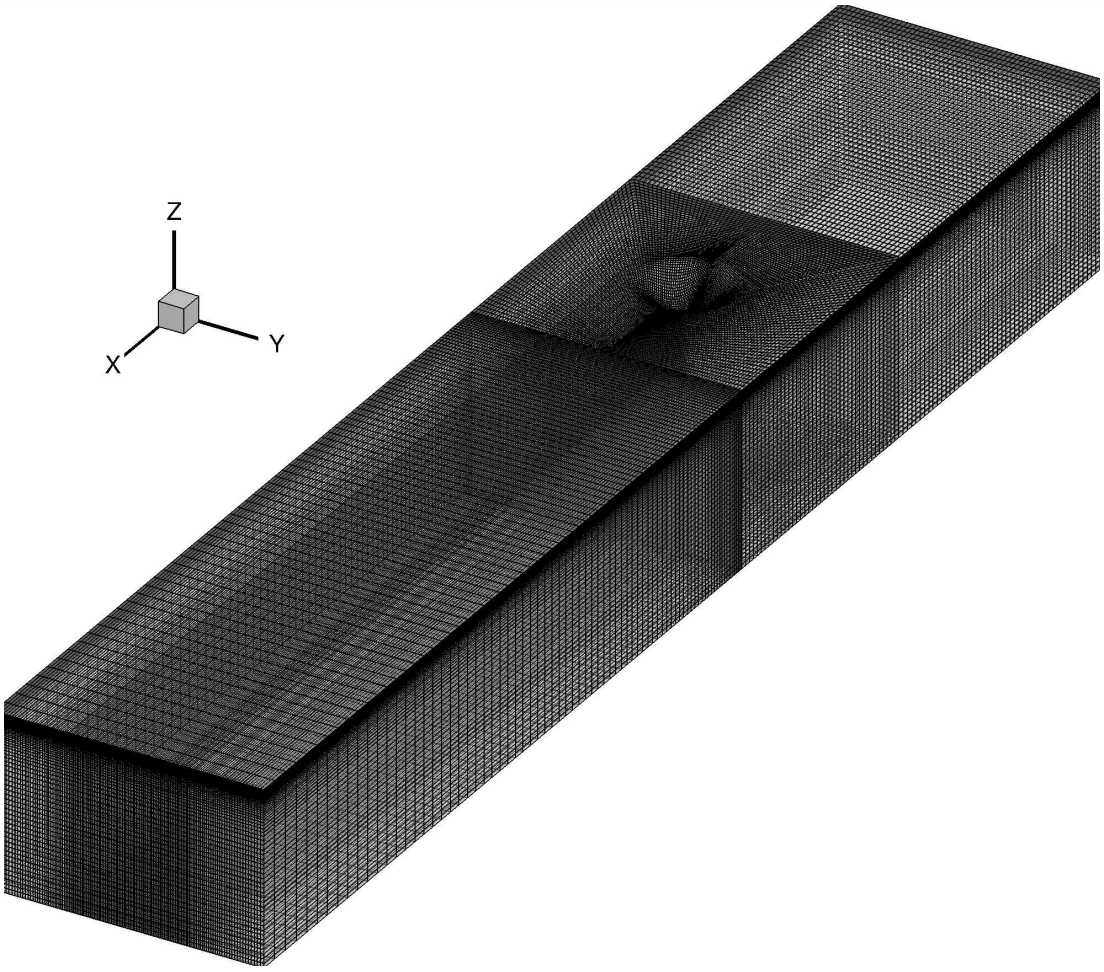

Figure 3. Full grid for FAITH. Grid is oriented for best view of lower surface with bump; flow is in positive x direction, as usual.

Case	Computation	Separation	Reattachment
1	Std. DES	0.64	1.34
2	MI $C_{DES} = 0.65$	0.66	1.19
3	MI $C_{DES} = 0.001333$	0.66	1.11
3a	MI-ns $C_{DES} = 0.001333$	0.66	1.11
4	MI $C_{DES} = 0.00125$	0.66	1.09
5	MI $C_{DES} = 0.001053$	0.66	1.08
—	Experiment	0.65	1.11

Table 1. Mean separation and reattachment points: Standard DES computation, model-invariant (MI) computations with various values of C_{DES} and model-invariant computation with no source terms (MI-ns).

flow (such as, perhaps, at the leading edge of the hump) that contributes to the generation of fluctuations. The vorticity-magnitude contours in Figure 7 show how successful such a computation is in generating and maintaining fluctuations. On the other hand, the contours of modelled turbulent kinetic energy in Figure 8 show the price paid for this success: the kinetic energy, and thus the eddy viscosity, are zero everywhere except near the wall and in the neighborhood of the separation point, pretty much eliminating any effect of the turbulence model in the separation bubble.

This compensation for numerical dissipation by reduction of the turbulent viscosity is certainly not proposed as a general solution to the problem of excess numerical dissipation, for it is far too crude, over-compensating in some parts of the flow and under-compensating in others. It also reduces the range of

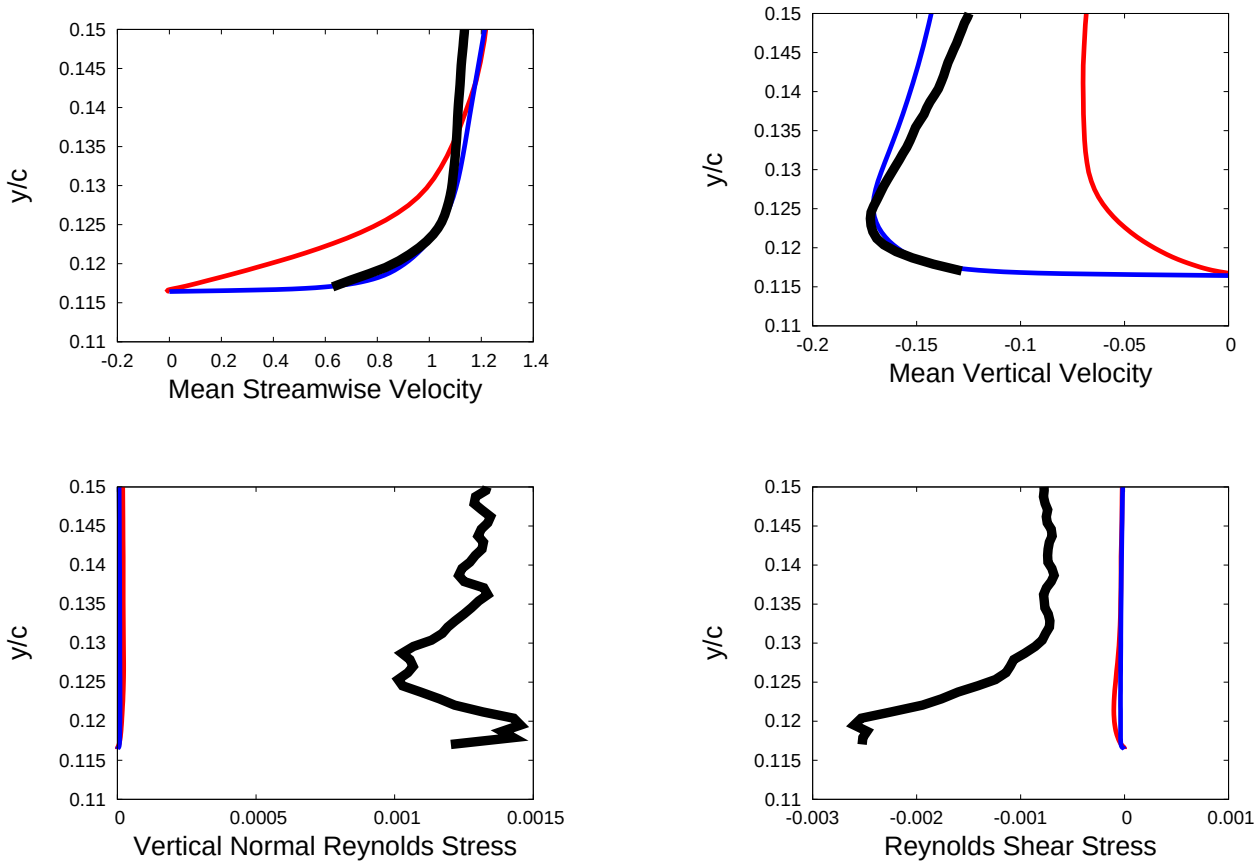

Figure 4. Comparison between standard DES (Case 1, red curve), model-invariant computation with $C_{DES} = 0.65$ (Case 2, blue curve) and experiment (black curve) at $x/c = 0.65$.

control the turbulence model has over the flow, making turbulence modelling less effective. Nevertheless, this device is useful as a diagnostic, since it helps to identify the reasons for the poor results at normal values of C_{DES}. It also leads to surprisingly good results, to be discussed next, which indicate how profitable solving these numerical problems could be.

Three computations with reduced C_{DES} were performed which yield separation bubbles that are approximately correct (Case 3), 4% too small (Case 4) and 7% too small (Case 5). (See Table 1.) As before, profiles of mean velocities and second-order moments are compared with experimental results at the separation point, within the separation bubble and at reattachment (Figures 9–11). Overall, agreement is fairly good for the computation with the correct separation-bubble length (Case 3); the others deviate slightly more. Some discrepancies in the mean velocities are seen which seem to increase in the aft-most profile and are probably due to grid deficiencies, particularly the nearness of the outflow boundary. While the normal Reynolds stresses are over-predicted, particularly at the rear of the bubble, the consistent agreement of the Reynolds shear stress is directly related to the correctness of the bubble-size prediction.

These profiles at select streamwise locations are instructive, but it is helpful to get a more complete picture of the generation and maintenance of the turbulent fluctuations by following Bentaleb et al.[46] in plotting the streamwise development of the peak resolved Reynolds shear stress (Figure 12). As this quantity is the contribution of the fluctuating velocities to the vertical component of the momentum flux past a given streamwise station, its development through separation, bubble and reattachment is intimately related to the correct prediction of the turbulence dynamics and the overall solution. All six of the solutions discussed in this section are compared in Figure 12 with experimental results. It is clear from this comparison that the fidelity of a computation's prediction of the reattachment point is directly related to the fidelity with which the Reynolds shear-stress evolution is predicted.

To evaluate the significance of the model-invariance terms, the best of the above computations (Case 3) is compared with an identical computation with these terms switched off (Case 3a). The profiles of mean

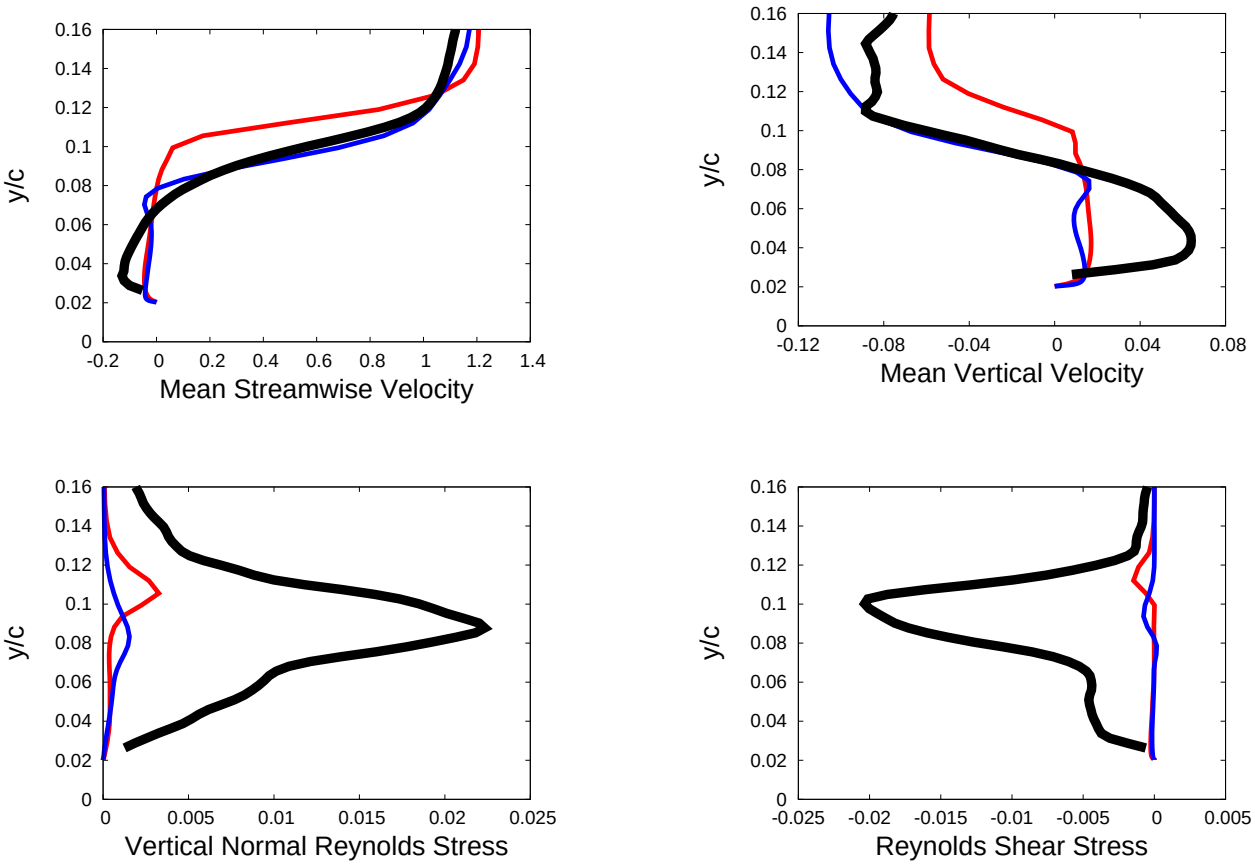

Figure 5. Comparison between standard DES (Case 1, red curve), model-invariant computation with $C_{DES} = 0.65$ (Case 2, blue curve) and experiment (black curve) at $x/c = 0.8$.

velocities and Reynolds stresses shown in Figures 13–15 indicate that these terms, in fact, have very little effect on the solution in the present situation. This suggests that the selected transition zone is sufficiently wide, and is sufficiently free of rapidly changing turbulence dynamics, that the model-invariance terms have a neglegible effect on the overall flow. As noted in Section II, the present approach differs significantly from existing work even without the model-invariance terms, because the gradual transition employed here is in marked contrast to the abrupt transition favored by other approaches.

Computations of the FAITH configuration were developed in similar fashion to those just discussed for the NASA hump. As before, a wide transition zone was selected, in the middle and upper portions of the wall boundary layer. Again, a significantly reduced C_{DES} was required to maintain fluctuations and, again, it is likely that instabilities at the leading edge of the hump were enhanced by the reduced dissipation (note separated flow at leading edge in Figure 16) and supplied the random forcing necessary to give good results in the neighborhood of the separation bubble. The computation yielded separation and reattachment points in good agreement with experiment. The analysis of the NASA hump results revealed the significance of the streamwise evolution of the peak Reynolds shear stress; Figure 17 shows the FAITH configuration exhibits similar behavior, with a rapid rise from nearly zero just after the separation point and then a gradual decline after reattachment. As in the hump case, the predicted peak Reynolds shear-stress evolution agrees fairly well with the experiment.

VI. Discussion

Two modifications to typical hybrid LES-RANS practice are involved in a model-invariant hybrid computation. The first, use of a gradual, continuous, blending of RANS and LES models in place of the more usual abrupt transition, was sufficient to yield good results in the test cases examined here. The second, the inclusion of model-invariance terms in the equations of motion that compensate for spurious changes

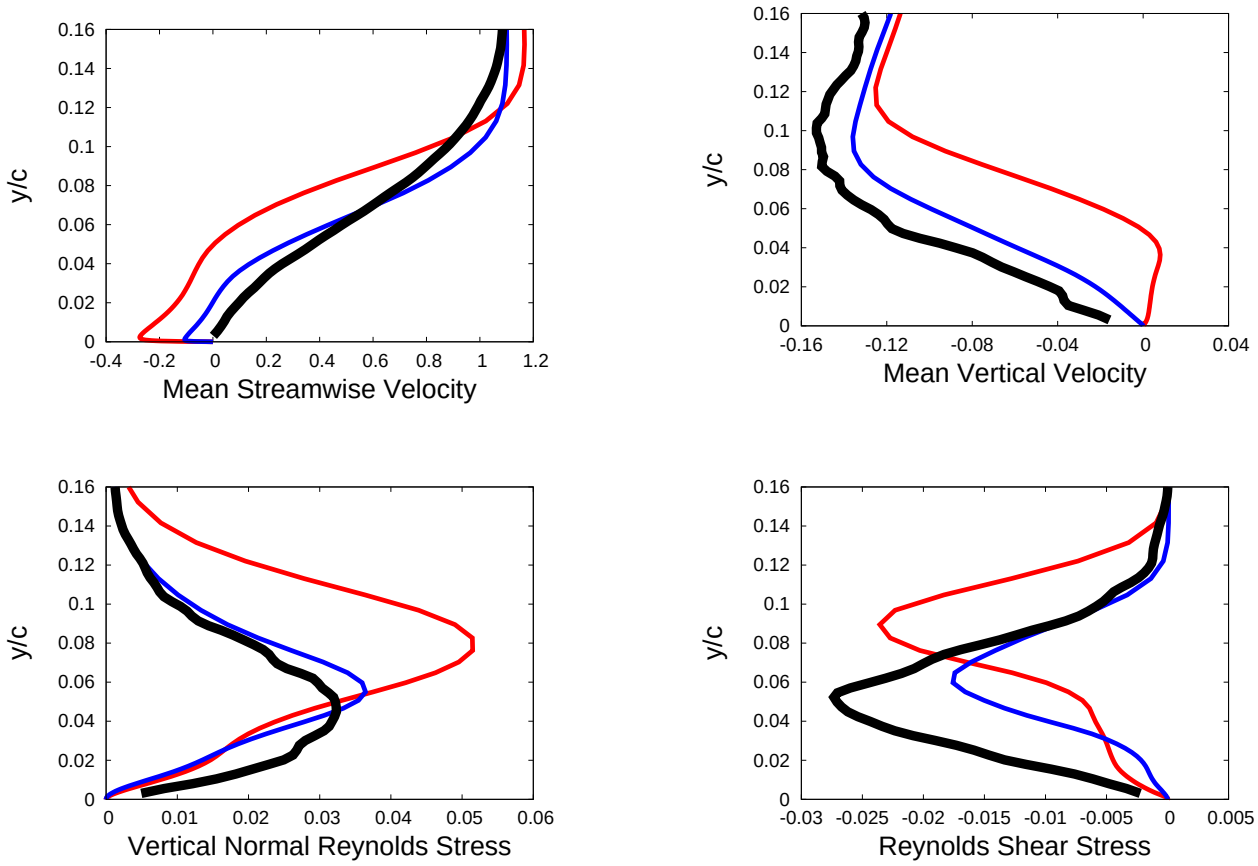

Figure 6. Comparison between standard DES (Case 1, red curve), model-invariant computation with $C_{DES} = 0.65$ (Case 2, blue curve) and experiment (black curve) at $x/c = 1.1$.

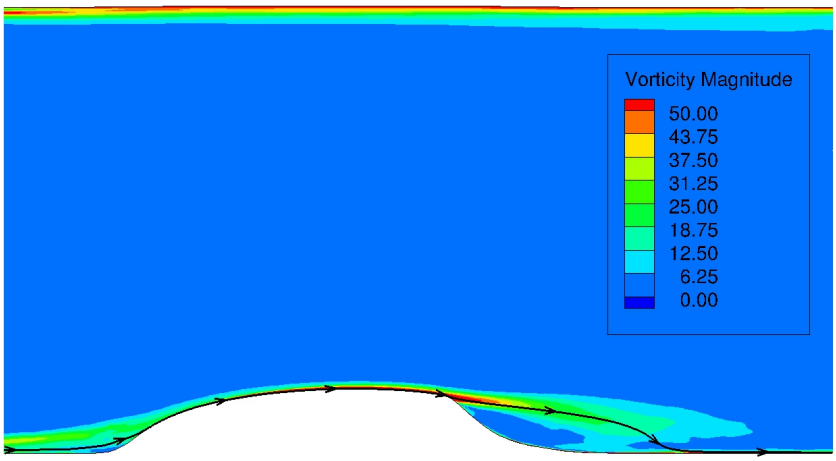

Figure 7. Vorticity magnitude for NASA hump. The dividing streamline outlines the separation bubble.

in flow variables due to changes in the model, was found to have neglegible effect. The model-invariance terms are products of model sensitivities and time and space derivatives of the blending parameter: the fact

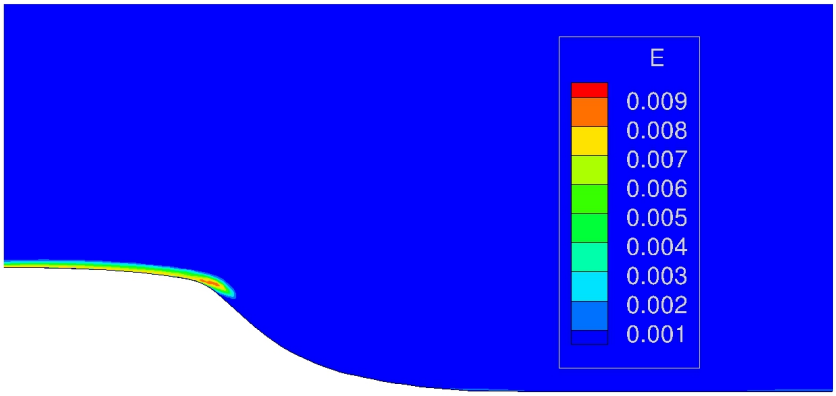

Figure 8. Modeled turbulent kinetic energy for NASA hump.

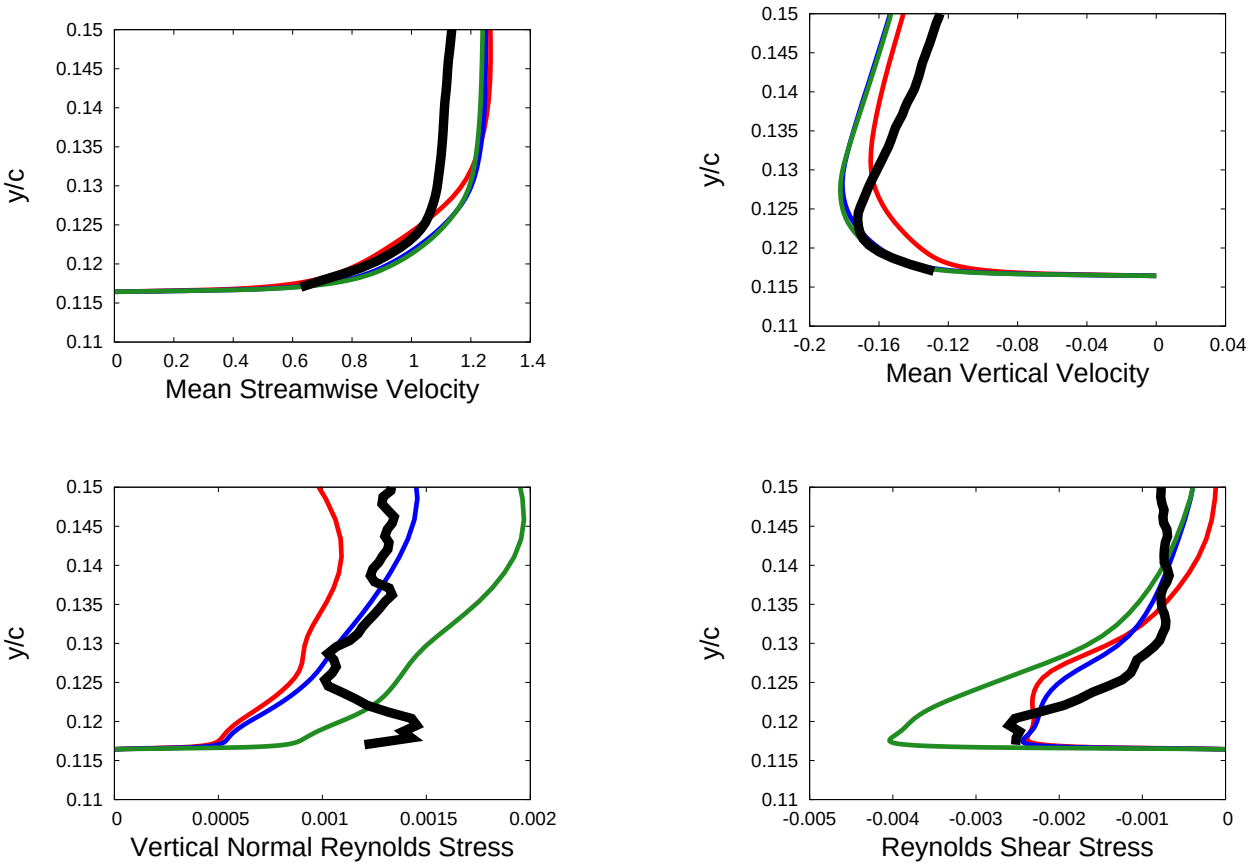

Figure 9. Comparison between model-invariant computations with $C_{DES} = 0.001333$ (Case 3, red curve), $C_{DES} = 0.00125$ (Case 4, blue curve), $C_{DES} = 0.001053$ (Case 5, green curve) and experiment (black curve) at $x/c = 0.65$.

that the terms are small is a consequence of using a wide transition zone placed so there is little overlap with regions of rapidly changing turbulence dynamics. The application of the model-invariant approach to periodic-hill flow[6] also showed relatively small effects due to the model-invariance terms, for the same reasons. In contrast, when applied to plane channel flow,[5] with narrower transition zones entirely in the log

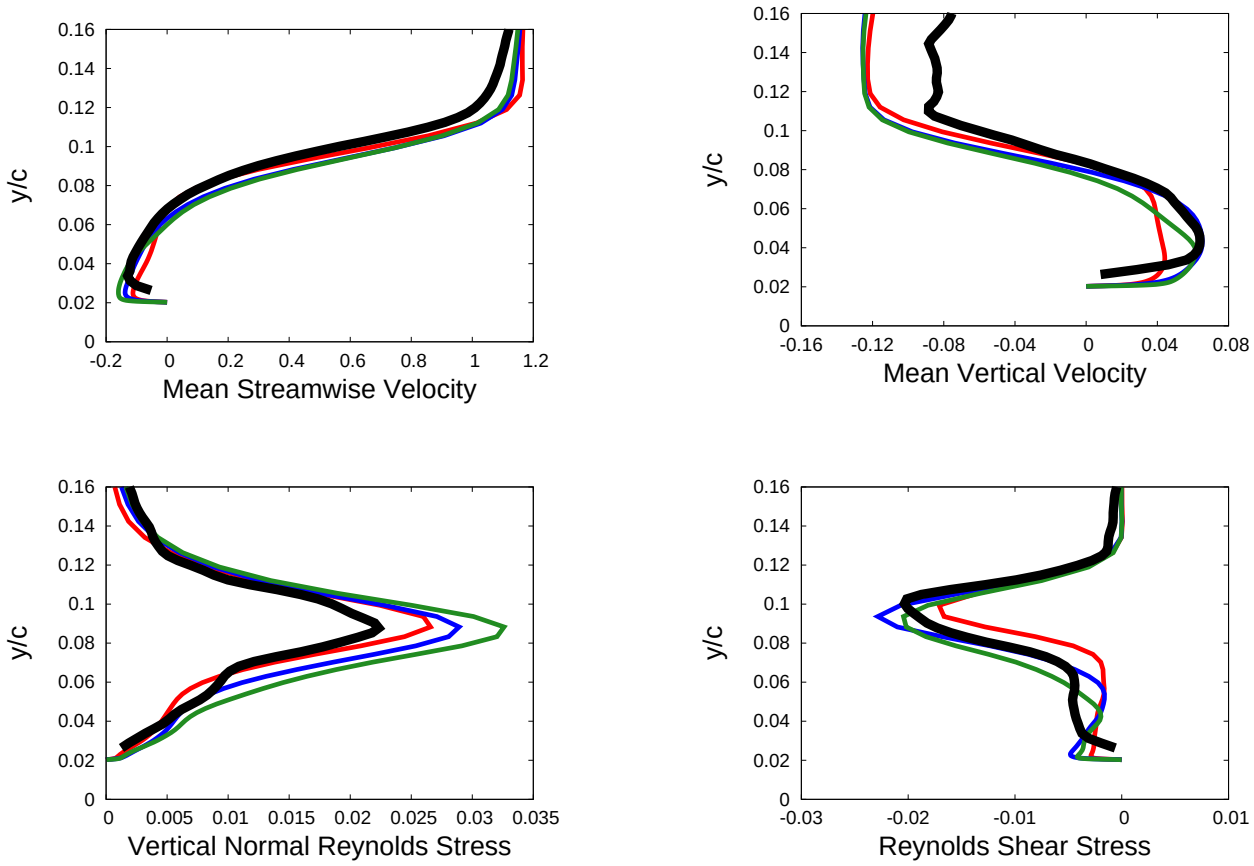

Figure 10. Comparison between model-invariant computations with $C_{DES} = 0.001333$ (Case 3, red curve), $C_{DES} = 0.00125$ (Case 4, blue curve) and $C_{DES} = 0.001053$ (Case 5, green curve) and experiment (black curve) at $x/c = 0.8$.

layer and in the vicinity of maximum turbulent kinetic energy production, the model-invariance terms were crucial in generating and maintaining the correct level of turbulent fluctuations and eliminating log-layer mismatch. These results suggest there are (at least) three kinds of computations: those for which existing hybrid schemes are successful without modification, those for which replacement of an abrupt transition by a gradual one yields a successful computation and those for which a gradual transition augmented by model-invariance terms is required for a successful computation.

The good results presented above were only possible through the device of significantly reducing the model constant C_{DES}. This is not proposed as a solution, but as a diagnostic revealing that the earlier poor solutions were the result of excessive dissipation. Successful results for this problem without reducing C_{DES} in a related investigation employing a finite-difference/spectral code also suggests the problem is algorithm-related. The central-differencing and solution filtering inviscid scheme implemented in VULCAN-CFD in this investigation helped a great deal, but it was not enough. Moderate refinement of the grid had little effect; extensive refinement should ultimately be successful, but at such computational cost that the test cases would be useless for future investigations into turbulence-model development and separated-flow physics. These findings are simply a consequence of the fact that the numerical requirements of hybrid LES-RANS computations are defined by LES, not RANS. The issues that arose in this work are not specific to VULCAN-CFD and will impede successful hybrid computations in any code that does not give a high level of control over numerical accuracy and dissipation.

Experimental results for both test cases examined in this paper show low turbulence levels just prior to separation, followed by a rapid rise at and just beyond separation. The successful hybrid computations discussed above were seen to capture this aspect of turbulence dynamics well, while the unsuccessful computations exhibited a much slower rise in turbulence levels. This suggests the streamwise evolution of the peak Reynolds shear stress (and similar quantities) can provide good global measures of turbulence dynamics in separated regions and provide good measures of how well computations reproduce those dynamics. Of the

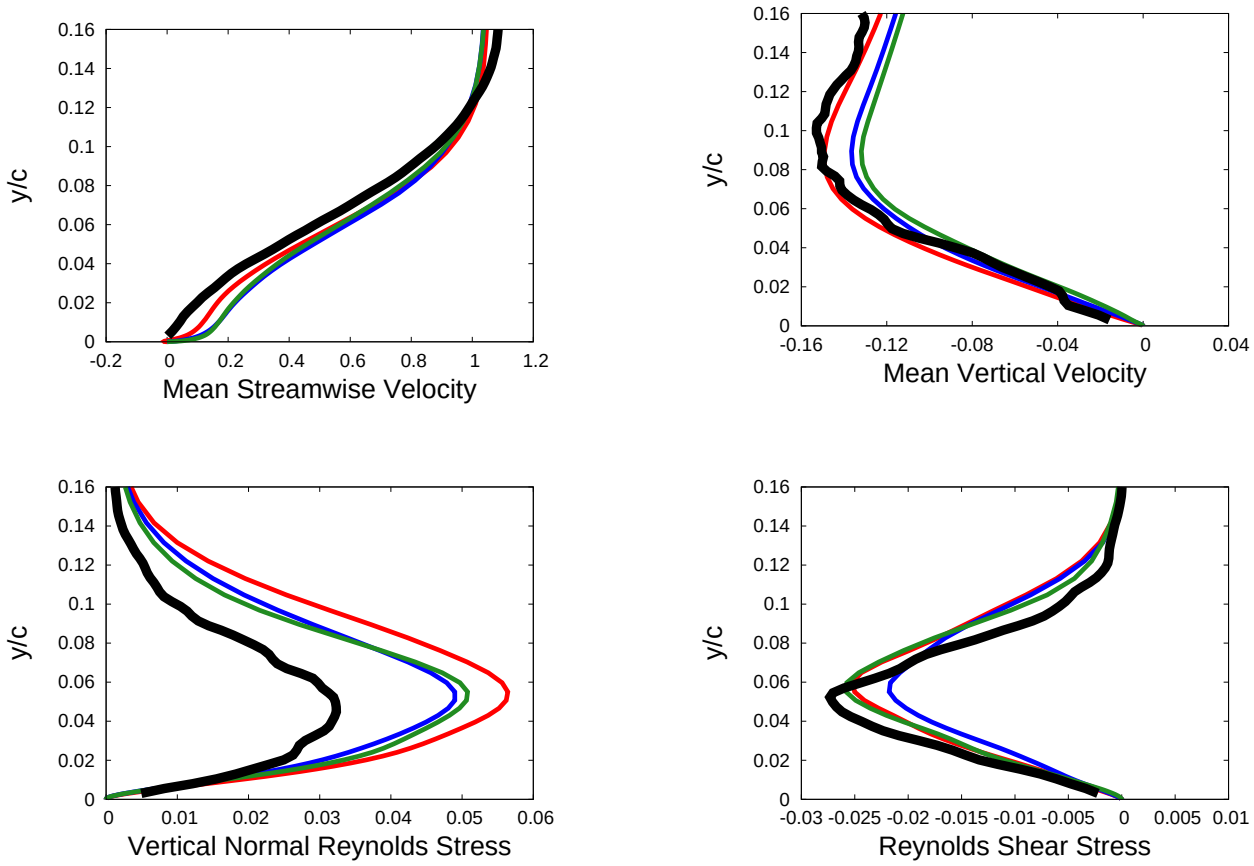

Figure 11. Comparison between model-invariant computations with $C_{DES} = 0.001333$ (Case 3, red curve), $C_{DES} = 0.00125$ (Case 4, blue curve), $C_{DES} = 0.001053$ (Case 5, green curve) and experiment (black curve) at $x/c = 1.1$.

hybrid computations of these test cases in the literature for which streamwise turbulence evolution information is available, Refs. 27 and 35 exhibited a slower rise then that shown by experiment, while Ref. 31's Reynolds shear-stress levels are too high in the forward part of the separation bubble. In each case, bubble size and other features were also predicted less well than in the present work. (Ref. 13 did not provide information about streamwise turbulence evolution, but presumably it was predicted quite accurately, given the accurate predictions of separation and reattachment.)

There are two principal conclusions to be drawn from these results. The first is that, with proper management of LES-RANS transitions via the model-invariant hybrid formulation, accurate results may be achieved with low computational costs. The second is that reliable hybrid computations are possible only with controlled, predictable levels of numerical accuracy and dissipation.

Acknowledgments

The assistance of J. White and R. Baurle in working with VULCAN-CFD was indispensable. Helpful comments on manuscript drafts by J. White, R. Baurle and B. Kleb are gratefully acknowledged. This work was funded by the Revolutionary Computational Aerosciences sub-project of the Transformational Tools and Technologies project of the Transformative Aeronautics Concepts Program within NASA's Aeronautics Research Mission Directorate.

References

[1]Rumsey, C., "Exploring a Method for Improving Turbulent Separated-Flow Predictions with k-ω Models," NASA TM–2009–215952.

[2]Greenblatt, D., Paschal, K. B., Yao, C.-S., Harris, J., Shaeffler, N. W., and Washburn, A. E., "Experimental Investigation of Separation Control, Part 1: Baseline and Steady Suction," *AIAA Journal*, Vol. 44, No. 12, 2006, pp. 2820–2830.

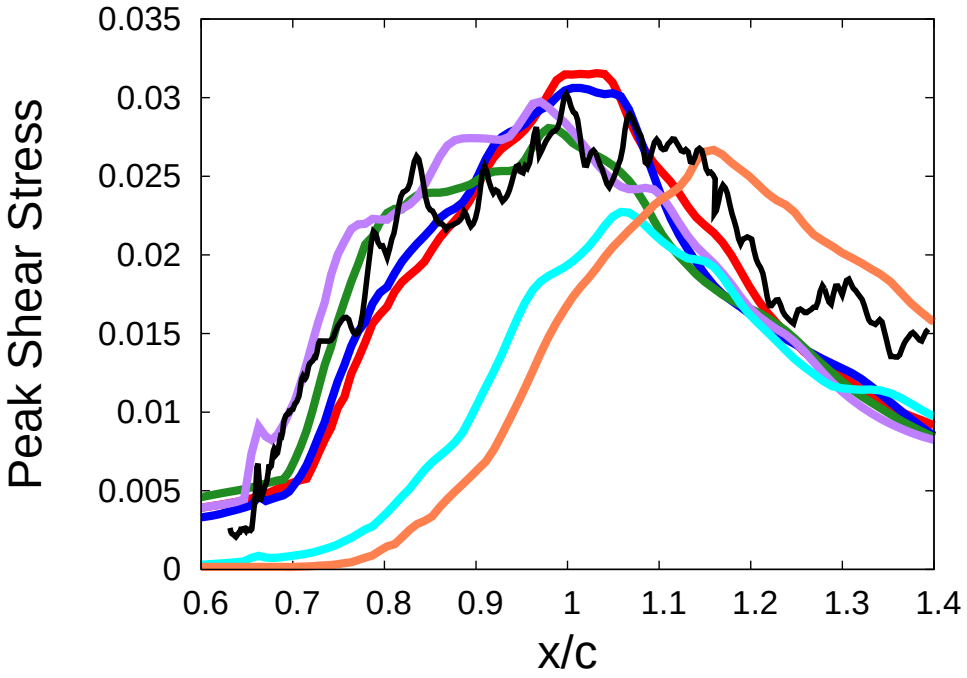

Figure 12. Peak shear stress for NASA hump as a function of streamwise position: model-invariant computations with $C_{DES} = 0.001333$ with (Case 3, red curve) and without (Case 3a, blue curve) model-invariance terms, with $C_{DES} = 0.00125$ (Case 4, green curve), with $C_{DES} = 0.001053$ (Case 5, purple curve), with $C_{DES} = 0.65$ (Case 2, cyan curve), standard DES computation (Case 1, orange curve) and experiment (black curve). The separation and reattachment points are at $x/c = 0.65$ and $x/c = 1.11$, respectively.

[3]Bell, J. H., Heineck, J. T., Zilliac, G., Mehta, R. D., and Long, K. R., "Surface and Flow Field Measurements on the FAITH Hill Model," *50th AIAA Aerospace Sciences Meeting*, 9–12 January 2012, Nashville, Tennessee, AIAA Paper 2012-0704.

[4]Woodruff, S. L., "Coupling Turbulence in Hybrid LES-RANS Techniques," *Seventh International Symposium on Turbulence and Shear-Flow Phenomena*, Ottawa, Canada, July 28–31, 2010.

[5]Woodruff, S. L., "A New Formulation for Hybrid LES-RANS Computations," 21st AIAA Computational Fluid Dynamics Conference, June 24-27, 2013, San Diego, CA, AIAA Paper 2013-2722.

[6]Woodruff, S., "Model-Invariant Hybrid LES-RANS Computation of Separated Flow Past Periodic Hills," in *Progress in Hybrid RANS-LES Modelling*, S. Girimaji et al. (eds.), *Notes on Numerical Fluid Mechanics and Multidisciplinary Design*, Vol. 130, Springer, 2015.

[7]VULCAN-CFD, http://vulcan-cfd.larc.nasa.gov, last accessed October 26, 2015.

[8]Shur, M. L., Spalart, P. R., Strelets, M. Kh. and Travin, A., "A hybrid RANS-LES approach with delayed-DES and wall-modeled LES capabilities," *Int. J. Heat and Fluid Flow*, Vol. 29, 2008, pp. 1638–1649.

[9]Choi, J.-I., Edwards, J. R. and Baurle, R. A., "Compressible Boundary Layer Predictions at High Reynolds Number using Hybrid LES/RANS Methods," *AIAA J.*, Vol. 47, No. 9, 2009, pp. 2179–2193.

[10]Gieseking, D. A., Choi, J.-I., Edwards, J. R. and Hassan, H. A., "Simulation of Shock/Boundary Layer Interactions Using Improved LES/RANS Models," *48th AIAA Aerospace Sciences Meeting*, January 4–7, 2010, Orlando, FL, AIAA Paper 2010-0111.

[11]Keating, A., De Prisco, G. and Piomelli, U., "Interface conditions for hybrid RANS/LES calculations," *Int. J. Heat and Fluid Flow*, Vol. 27, 2006, pp. 777–788.

[12]Davidson, L. and Billson, M., "Hybrid LES-RANS using synthesized turbulent fluctuations for forcing in the interface region," *Int. J. Heat and Fluid Flow*, Vol. 27, 2006, pp. 1028–1042.

[13]Shur, M. L., Spalart, P. R., Strelets, M. K. and Travin, A. K., "Synthetic Turbulence Generators for RANS-LES Interfaces in Zonal Simulations of Aerodynamic and Aeroacoustic Problems," *Flow Turbulence Combust.*, Vol. 93, 2014, pp. 63–92.

[14]Germano, M., "Properties of the Hybrid RANS/LES Filter," *Theoretical and Computational Fluid Dynamics*, Vol. 17, 2004, pp. 225–231.

[15]Hamba, F., "Log-layer mismatch and commutation error in hybrid RANS/LES simulation of channel flow," *Int. J. Heat and Fluid Flow*, Vol. 30, 2009, pp. 20–31.

[16]Sanchez-Rocha, M. and Menon, S., "The Compressible Hybrid RANS/LES Formulation Using an Additive Operator," *Journal of Computational Physics*, Vol. 228, 2009, pp. 2037–2062.

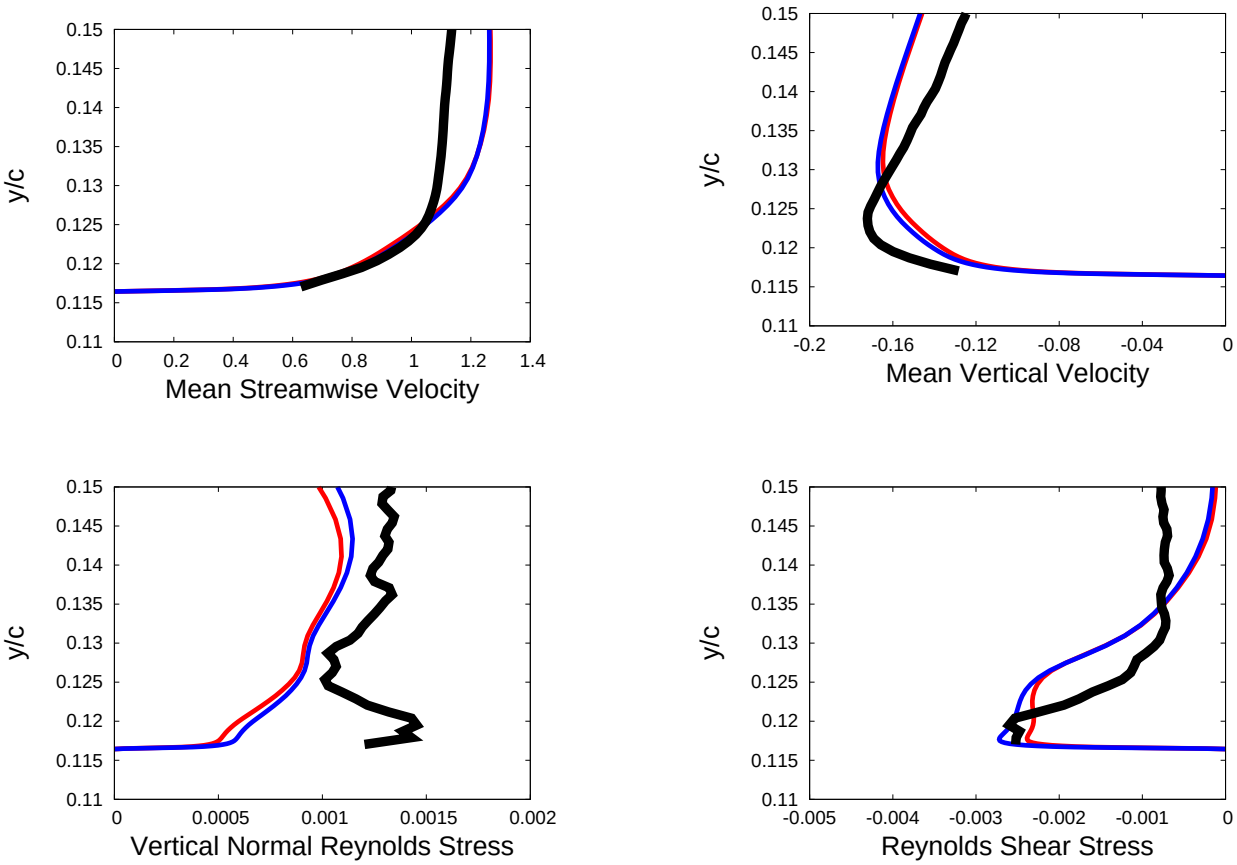

Figure 13. Comparison between model-invariant computations with $C_{DES} = 0.001333$ with (Case 3, red curve) and without (Case 3a, blue curve) model-invariance terms and experiment (black curve) at $x/c = 0.65$.

[17]Sanchez-Rocha, M. and Menon, S., "An Order-of-Magnitude Approximation for the Hybrid Terms in the Compressible Hybrid RANS/LES Governing Equations," *Journal of Turbulence*, Vol. 12, 2011, N16.

[18]Rajamani, B. and Kim, J., "A Hybrid-Filter Approach to Turbulence Simulation," *Flow Turbulence Combust.*, Vol. 85, 2010, pp. 421–441.

[19]Wallin, S. and Girimaji, S., "Commutation Error Mitigation in Variable-Resolution PANS Closure: Proof of Concept in Decaying Isotropic Turbulence," *6th AIAA Theoretical Fluid Mechanics Conference*, June 27–30, 2011, Honolulu, HI, AIAA Paper 2011-3105.

[20]Wang, M. and Moin, P., "Dynamic wall modeling for large-eddy simulation of complex turbulent flows," *Physics of Fluids*, Vol. 14, No. 7, 2002, pp. 2043–2051.

[21]Medic, G., Templeton, J. A., and Kalitzin, G., "A Formulation for Near-Wall RANS/LES Coupling," *International Journal of Engineering Science*, Vol. 44, 2006, pp. 1099–1112.

[22]Breuer, M., Jaffrezic, B., and Arora, K., "Hybrid LES-RANS Technique Based on a One-Equation Near-Wall Model," *Theoretical and Computational Fluid Dynamics*, Vol. 22, 2008, pp. 157–187.

[23]Park, G. I. and Moin, P., "An improved dynamic non-equilibrium wall-model for large eddy simulation," *Physics of Fluids*, Vol. 26, 2014, 015108.

[24]Rumsey, C. L., Gatski, T. B., Sellers III, W. L., Vatsa, V. N., and Viken, S. A., "Summary of the 2004 Computational Fluid Dynamics Validation Workshop on Synthetic Jets," *AIAA Journal*, Vol. 44, No. 2, 2006, pp. 194–205.

[25]Capizzano, F., Catalano, P., Marongiu, C., and Vitagliano, P. L., "U-RANS Modelling of Turbulent Flows Controlled by Synthetic Jets," *35th AIAA Fluid Dynamics Conference and Exhibit,* 6–9 June 2005, Toronto, Ontario, Canada, AIAA Paper 2005-5015.

[26]Rumsey, C. L., "Reynolds-Averaged Navier-Stokes Analysis of Zero Efflux Flow Control over a Hump Model," *44th AIAA Aerospace Sciences Meeting and Exhibit,* 9–12 January 2006, Reno, Nevada, AIAA Paper 2006-1114.

[27]Krishnan, V., Squires, K. D., and Forsythe, J. R., "Prediction of Separated Flow Characteristics over a Hump," *AIAA Journal*, Vol. 44, No. 2, 2006, pp. 252–262.

[28]Avdis, A., Lardeau, S., and Leschziner, M., "Large Eddy Simulation of Separated Flow over a Two-Dimensional Hump with and without Control by Means of a Synthetic Slot-Jet," *Flow Turbulence Combust.*, Vol. 83, 2009, pp. 343–370.

[29]You, D., Wang, M., and Moin, P., "Large-Eddy Simulation of Flow over a Wall-Mounted Hump with Separation Control," *AIAA Journal*, Vol. 44, No. 11, 2006, pp. 252–262.

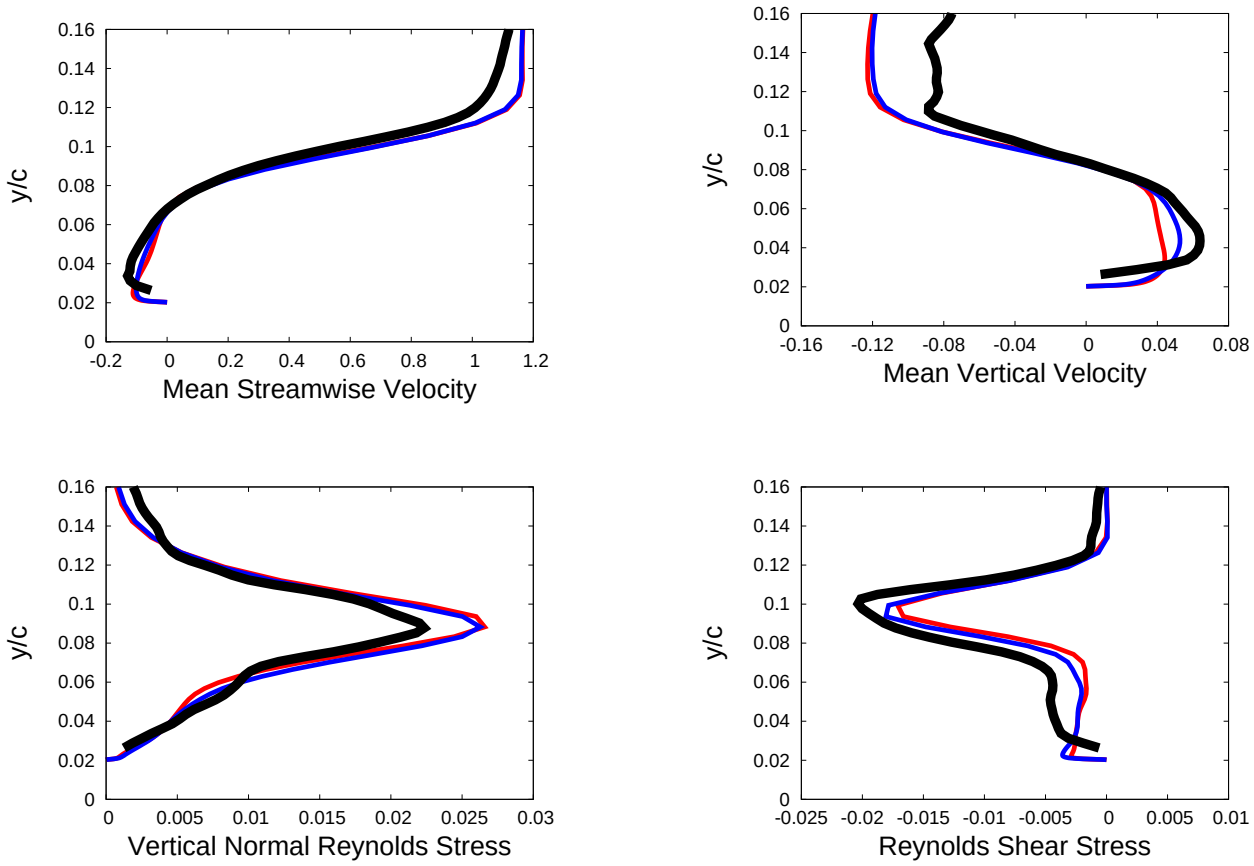

Figure 14. Comparison between model-invariant computations with $C_{DES} = 0.001333$ with (Case 3, red curve) and without (Case 3a, blue curve) model-invariance terms and experiment (black curve) at $x/c = 0.8$.

[30]Morgan, P. E., Rizzetta, D. P., and Visbal, M. R., "Large-Eddy Simulation of Separation Control for Flow over a Wall-Mounted Hump," *AIAA Journal*, Vol. 45, No. 11, 2007, pp. 2643–2660.

[31]Higuera, D., Sekhar, S., Mansour, N. N., Razi, P., and Girimaji, S., "PANS Simulations of Turbulent Separated Flow over a Wall-Mounted Hump," *22nd AIAA Computational Fluid Dynamics Conference*, 22–26 June 2015, Dallas, TX, AIAA Paper 2015-2463.

[32]Sekhar, S., Mansour, N. N., and Higuera, D., "Implicit LES of turbulent, separated flow: wall-mounted hump configuration," *22nd AIAA Computational Fluid Dynamics Conference*, 22–26 June 2015, Dallas, TX, AIAA Paper 2015-1966.

[33]Olsen, M. E., Lillard, R. P., and Murman, S. M., "Prediction of Large Separations with Reynolds Stress Models," *21st AIAA Computational Fluid Dynamics Conference*, June 24-27, 2013, San Diego, CA, AIAA Paper 2013-2720.

[34]Rodio, J. J., Patton, C. H., Xiao, X., and Hassan, H. A., "Simulation of the FAITH Hill Experiment using a Reynolds Stress Model," *44th AIAA Fluid Dynamics Conference*, 16–20 June 2014, Atlanta, GA, AIAA Paper 2014-2210.

[35]Yin, Z., Reddy, K. R., and Durbin, P. A., "On the dynamic computation of the model constant in delayed detached eddy simulation," *Physics of Fluids*, Vol. 27, 2015, 025105.

[36]Nikitin, N. V., Nicoud, F., Wasistho, B., Squires, K. D., and Spalart, P. R., "An approach to wall modelling in large-eddy simulations," *Physics of Fluids*, Vol. 12, No. 7, 2000, pp. 1629–1632.

[37]Speziale, C. G., "Turbulence Modeling for Time-Dependent RANS and VLES: A Review" *AIAA J.*, Vol. 36, No. 2, 1998, pp. 173–184.

[38]Spalart, P. R., "Detached-Eddy Simulation," *Annual Review of Fluid Mechanics*, Vol. 41, 2009, pp. 181–202.

[39]Strelets, M., "Detached Eddy Simulation of Massively Separated Flows," *39th AIAA Aerospace Sciences Meeting*, January 8–11, 2001, Reno, NV, AIAA Paper 2001-0879.

[40]Menter, F. R., "Two-Equation Eddy-Viscosity Turbulence Models for Engineering Applications," *AIAA J.*, Vol. 32, No. 8, 1994, pp. 1598–1605.

[41]White, J. A., Baurle, R. A., Fisher, T. C., Quinlan, J. R. and Black, W. S., "Low-dissipation Advection Schemes Designed for Large Eddy Simulations of Hypersonic Propulsion Systems," *48th AIAA/ASME/SAE/ASEE Joint Propulsion Conference and Exhibit*, July 30 – August 1, 2012, Atlanta, GA, AIAA Paper 2012–4263.

[42]Woodruff, S., "Coupled RANS/LES for SOFIA Cavity Acoustic Prediction," *48th AIAA Aerospace Sciences Meeting*, 4–7 January 2010, Orlando, Florida, AIAA Paper 2010-1202.

[43]Visbal, M. R. and Gaitonde, D. V., "On the Use of Higher-Order Finite-Difference Schemes on Curvilinear and Deforming Meshes," *Journal of Computational Physics*, Vol. 181, 2002, pp. 155–185.

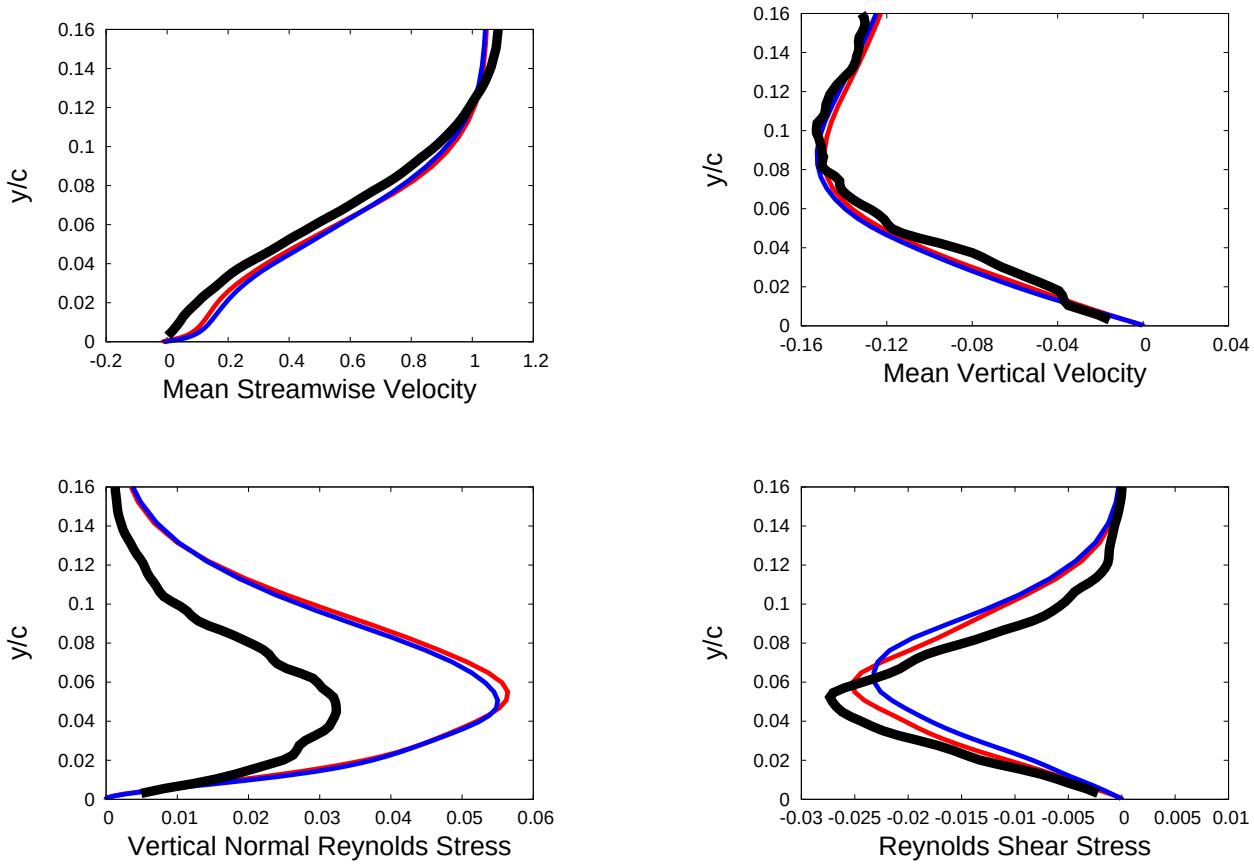

Figure 15. Comparison between model-invariant computations with $C_{DES} = 0.001333$ with (Case 3, red curve) and without (Case 3a, blue curve) model-invariance terms and experiment (black curve) at $x/c = 1.1$.

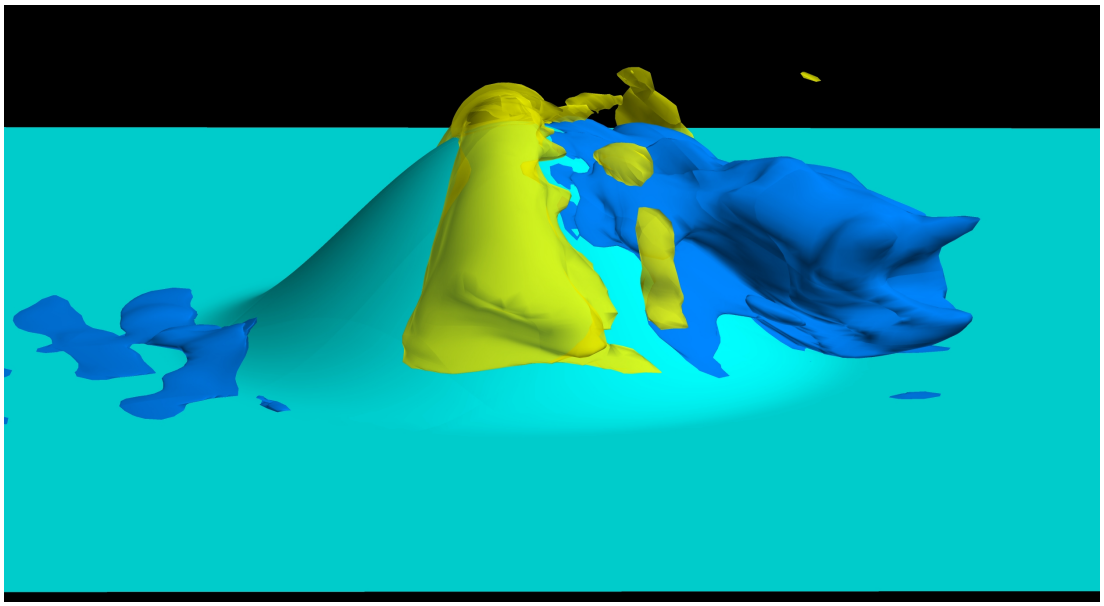

Figure 16. Instantaneous isovelocity surfaces for FAITH. Dark blue indicates flow-reversed regions; yellow indicates high-speed region where turbulent fluctuations are generated near separation.

[44]Colonius, T., "Modeling Artificial Boundary Conditions for Compressible Flow," *Annual Review of Fluid Mechanics*, Vol. 36, 2004, pp. 315–345.

[45]Travin, A., Shur, M., Strelets, M., and Spalart, P., "Detached-Eddy Simulations Past a Circular Cylinder," *Flow,*

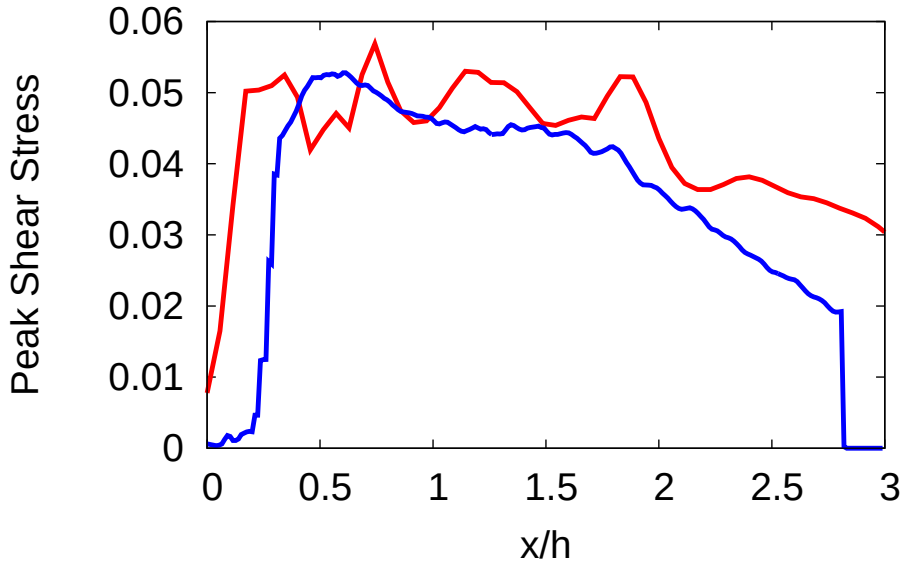

Figure 17. FAITH: Peak Reynolds shear-stress magnitudes at positions downstream of hilltop $(x/h = 0)$**. Computation (red curve), experiment (blue curve). Separation and reattachment points are at** $x/h = 0.23$ **and** $x/h = 1.82$**, respectively.**

Turbulence and Combustion, Vol. 63, 1999, pp. 293–313.

[46]Bentaleb, Y., Lardeau, S. and Leschziner, M. A., "Large-eddy simulation of turbulent boundary-layer separation from a rounded step," *Journal of Turbulence*, Vol. 13, 2012, N4.